THE JOURNAL OF BIOLOGICAL CHEMISTRY VOL. 282, NO. 9, pp. 6668–6676, March 2, 2007

IDI2, a Second Isopentenyl Diphosphate Isomerase in Mammals*

Received for publication, November 27, 2006, and in revised form, January 2, 2007 Published, JBC Papers in Press, January 3, 2007, DOI 10.1074/jbc.M610922200

Daun B. Clizbe, Michelle L. Owens, Kimberly R. Masuda, Janis E. Shackelford, and Skaidrite K. Krisans[1]

From the Department of Biology, San Diego State University, San Diego, California 92182

We recently described the identification of a novel isopentenyl diphosphate isomerase, IDI2 in humans and mice. Our current data indicate that, in humans, IDI2 is expressed only in skeletal muscle. Expression constructs of human IDI2 in *Saccharomyces cerevisiae* can complement isomerase function in an *idi1*-deficient yeast strain. Furthermore, IDI2 has the ability to catalyze the isomerization of [^{14}C]IPP to [^{14}C]DMAPP. Enzyme kinetic analysis of partially purified IDI2 demonstrate the novel isozyme has a maximal relative specific activity of $1.2 \times 10^{-1} \pm 0.3$ μmol min^{-1} mg^{-1} at pH 8.0 with a K_m^{IPP} value of 22.8 μM IPP. Both isozymes, IDI1 and IDI2 are localized to the peroxisome by a PTS1-dependent pathway. Finally, our data suggest that IDI2 is regulated independently from IDI1, by a mechanism that may involve PPARα.

Isoprenoids and isoprenoid-derived compounds play an essential role in all living systems. They provide a necessary function in the organization of many biological systems including membrane structure, signal transduction, and redox chemistry. Several of the important end products of the isoprenoid biosynthetic pathway include: prenylated proteins, dolichols, vitamins A, D, E, and K, steroid hormones, carotenoids, bile acids, and cholesterol (1). In addition, this complex pathway also produces farnesyl diphosphate (FPP)[2] and geranyl-geranyl diphosphate (GGPP), compounds required for the isoprenylation of various G proteins (2).

All isoprenoids are derived from the 5-carbon isoprene defined by isopentenyl diphosphate (IPP) and its highly electrophilic isomer dimethylallyl diphosphate (DMAPP). The enzyme isopentenyl diphosphate isomerase (IDI1; EC 5.3.3.2) transforms unreactive IPP into its reactive isomer DMAPP by the concerted addition and abstraction of protons at C-4. These two isomers are the building blocks for the successive head-to-tail condensation reactions that result in the synthesis of geranyl diphosphate (GPP, C_{10}) FPP (C_{15}) and ultimately, non-sterol products and cholesterol (3).

IDI1 first identified in *Saccharomyces cerevisiae* (4) has since been characterized in numerous organisms including humans. Most recently, IDI1 has been identified in hamster and rat where it was shown to localize to the peroxisome by a Pex-5p-dependent PTS1 mechanism (5).

Analysis of IDI1 in *S. cerevisiae* revealed two catalytically active amino acids, Cys^{139} and Glu^{207}. Mutagenesis analysis in the yeast enzyme demonstrated that a C139S mutation resulted in a significant reduction in isomerase activity whereas a Cys to Val or Ala change at this site abolished activity completely (6).

Several examples of multiple IDI isozymes have been reported in plants and algae. In *Nicotiana tobacum*, the two IDI isozymes are regulated at the transcriptional level under a variety of environmental conditions (7). Similar duplications exist in *Cinchona robusta* and the green alga *Hematococcus pluvialis.* Additionally, multiple isozymes of IDI have been identified in higher eukaryotes *Sus domesticus* and *Gallus gallus*. In all cases the isozymes maintain specialized functions by different expression patterns, subcellular localization, and susceptibility to inhibitors (8, 9).

We previously reported a detailed phylogenetic and structural analysis of IDI2 (10). Molecular modeling suggested that IDI2 is likely to perform functionally as an isomerase despite a Ser to Cys change within the putative active site. In the current study we present the biochemical and functional characterization of IDI2 in mammals. Our data illustrate that IDI2 has a distinct tissue expression pattern, has functional isomerase activity *in vivo*, a unique kinetic profile, and is targeted to the peroxisome by a PTS1-dependent pathway. Moreover, our results suggest that IDI2 in mice is regulated in an independent manner from its isozyme IDI1 and may play a significant role in isoprenoid metabolism in skeletal muscle.

EXPERIMENTAL PROCEDURES

Northern Blot Analysis—Human multiple tissue Northern blots were purchased from Clontech. Each blot contained ~2 μg of poly(A)$^+$RNA. Hybridizations were performed with [α-^{32}P]dCTP-labeled probes. The [α-^{32}P]dCTP-labeled probes consisted of the 687-bp IDI1 and 684-bp IDI2 open reading frames. Standard procedures were followed for hybridization and washing. Membranes were exposed to a Phosphorimager screen (Molecular Dynamics). Dr. D. Shoemaker, Merck Pharmaceuticals, provided the real-time PCR data of human tissues.

RNA Isolation—Cells for RNA isolation were harvested by trypsinization and pelleted by centrifugation at 1000 rpm for 10 min at 4 °C. The pellet was flash-frozen in liquid nitrogen. RNA

* This work was supported in part by National Institutes of Health Grants DK58238 and DK58040. The costs of publication of this article were defrayed in part by the payment of page charges. This article must therefore be hereby marked "*advertisement*" in accordance with 18 U.S.C. Section 1734 solely to indicate this fact.

[1] To whom correspondence should be addressed: Dept. of Biology, San Diego State University, San Diego, CA 92182. Tel.: 619-594-5368; Fax: 619-594-5676; E-mail: skrisans@sciences.sdsu.edu.

[2] The abbreviations used are: FPP, farnesyl diphosphate; IDI, isopentenyl diphosphate isomerase; PPARα, peroxisome proliferator-activated receptor α; IPP, isopentenyl diphosphate; DMAPP, dimethylallyl diphosphate; QRT-PCR, quantitative real-time PCR; RT, reverse transcriptase; EGFP, enhanced green fluorescent protein; MES, 4-morpholineethanesulfonic acid.

was isolated using TRIzol (Invitrogen) according to the manufacturer's protocol. RNA isolation from murine muscle was performed on flash-frozen tissue with RNeasy Fibrous Tissue Mini kit (Qiagen), according to the manufacturer's protocol.

cDNA Synthesis—cDNA synthesis was performed using SuperScript III (Invitrogen), Oligo(dT) primer (Invitrogen), and total RNA according to the manufacturer's protocol. The transcription step was performed at 50 °C for 60 min.

Yeast Expression Vectors—Human IDI1 and IDI2 cDNAs were amplified by reverse transcriptase PCR (RT-PCR). Amplification products were cloned into pYES2.1/V5-His-TOPO vector (Invitrogen). pYES2.1/V5-His-TOPO contains the *URA3* gene for selection in yeast and 2-μ origin for high copy maintenance. TOPO cloning reaction was prepared according to the manufacturer's recommendation using 1 μl each of the amplification products. 3 μl of each ligation reaction was used to transform One Shot Top 10 F′ (Invitrogen)-competent *Escherichia coli*. Colonies were selected on LB kanamycin (50 μg/ml) and recombinant plasmids isolated using Qiagen Miniprep Plasmid Isolation kit. Recombinant plasmids were screened by PCR with forward primers to the Gal1 region of pYES2.1/V5-His-TOPO (5′-AATSTSCCTCTATACTTTA-ACGTC-3′) and reverse primers to the 3′-end of either IDI1 or IDI2, 5′-CATTTACCTCGAGATTCACATTCTG-3′ or 5′-CTCGAGGGCCTCTCACACTCTG-3′. Positive recombinants were verified by DNA sequencing in triplicate (Micro-CoreFacility, San Diego State University, San Diego, CA).

Plasmid Shuffle—pYESIDI1 and pYESIDI2 were shuffled into haploid *S. cerevisiae* IDI1 deletion strain FH2–5b (generous gift of Dr. C. Dale Poulter, University of Utah, Salt Lake City, UT) by methods described previously (11) with few modifications. pYESIDI1 and pYESIDI2 were transformed into competent FH2–5b by the LiAc/TE/PEG method (Invitrogen). No pYESIDI1 double transformants were recovered. Following incubation at 30 °C for 3 days on solid SG -ura-leu-lys media, pYES IDI2 double transformants were washed from plates in SG (20% galactose) -ura-leu-lys media containing α-AA (3 mg/ml) transferred to α-AA-20% galactose (3 mg/ml) solid media plates and incubated at 30 °C for 72 h. Surviving colonies were then replica-plated on the same medium or solid α-AA medium containing glucose as the sole carbon source. This method selects for those colonies able to survive when the shuffled gene is actively transcribed but perishes when transcription is repressed by glucose. This method allowed the identification of true IDI2-positive shuffle transformants.

Yeast Colony PCR—Colonies shown to survive on α-AA medium including galactose but not on α-AA medium including glucose were resuspended in 20 μl of dH_20. 1 μl of a 1:10 dilution of these resuspensions were used in a 50-μl PCR reaction using pYes 2.1Gal1 forward primer 5′-AATATACCTC-TATACTTTAACGTC-3′ and IDI2 reverse primer 5′-CACT-CTGTGTATTTTGTGAAG-3′ (pYes 2.1IDI2) or pRS317IDI1 forward 5′-GTAATACGACTCACTATAGG-3′ and pRS317IDI1 reverse 5′-CCTCACTAAAGGGAACAAAAG-3′. PCR conditions were 95° 5 min (1 cycle), 94° 30 s, 55° 45 s, 72° 1 min (35 cycles) 72° 5 min. PCR products were analyzed by agarose gel electrophoresis.

hIDI2 Partial Purification—IDI2-expressing yeast cultures were centrifuged at 5000 rpm to pellet. Pellets were washed 2× in 5 mM Hepes, 10% glycerol, pH 7.0, and processed immediately or frozen at −70 °C. The remaining procedures were performed at 4 °C or on ice. Frozen pellets were thawed, rinsed with 5 mM Hepes, 10% glycerol, 10 mM dithiothreitol including protease inhibitors (Roche Protease Complete mini tablet). Acid-washed glass beads (Sigma) were pre-rinsed with 5 mM HEPES, 10% glycerol plus protease inhibitors. Yeast pellet suspension was added and homogenized by repeated cycles of vortexing and chilling in an ice water bath (30 s each, 5 cycles). The homogenate was centrifuged (Bio-Rad, microcentrifuge) 3 min at 4 °C, and the supernatant collected. The homogenization procedure was repeated for a total of three times. Supernatants were brought to 55% by addition of solid ultra-pure ammonium sulfate (ICN) Precipitating proteins were removed by centrifugation, and the supernatant was brought to 75% ammonium sulfate. Precipitating proteins were collected, resuspended in buffer plus 0.5 mM benzamidine, 0.1 mM Pefabloc, 100 μM leupeptin, 5 μg/ml pepstatin A, 1.28 μg/ml aprotinin, and dialyzed overnight at 4 °C. Samples were collected and diluted with 10% glycerol and applied to a DEAE cellulose column equilibrated in buffer only. The binding proteins were eluted with a 0–0.5 M KPO_4 gradient in buffer without protease inhibitors. Fractions containing IDI activity were pooled, diluted with water, and reapplied to a new DEAE column, and eluted with 0.5 M KPO_4 to concentrate. The concentrated fractions were applied to a Sephacryl S-200 (Sigma) column in 5 mM Hepes, 10% glycerol, 10 mM dithiothreitol, and fractions containing IDI activity located by enzymatic assay.

SDS-PAGE and Western Blotting Analysis—SDS-PAGE was carried out on NuPAGE Novex Bis-Tris 1.0 mm gel in MES SDS Running Buffer (Invitrogen) under reducing conditions, then electrotransferred onto a nitrocellulose membrane (Millipore) in NuPAGE transfer buffer using a XCell II Blot module(Invitrogen). Bound antibody was revealed by the addition of Western Lightning Chemiluminescence Reagent PLUS (PerkinElmer) substrate.

Isomerase Activity Assay—Isomerase activity was determined by a modified version of the assay as described by Satterwhite (12). The reaction was initiated by adding enzyme to a prewarmed assay mixture followed by incubation at 37 °C for 10 min. The reaction was terminated by adding 0.4 ml of 25% concentrated HCl in MeOH. 0.05 ml of [^{3}H]FPP in 70% EtOH, 25 mM NH_4HCO_3 was added as a standard, followed by incubation at 37 °C for 10 min. Each sample was extracted twice with 2.0-ml aliquots of petroleum ether. Measurements of isomerase activity were performed in triplicate and determined to be linear for all protein concentrations and time of incubation.

EGFP Fusion Constructs—Full-length coding regions for human IDI1and IDI2 were amplified by PCR using oligonucleotide primers that introduced unique 5′ BglII and 3′ KpnI restriction sites, IDI1 forward 5′-CCCATAGATCTGATCA-GACATTTTGTAATGATG-3′, IDI2 forward 5′-AGGTCGG-GTCAGATCTAGCAGCTAT-3′, IDI1 Reverse 5′-GTAATC-AGGTACCTACATATTCAC-3′ IDI2 Reverse 5′-CATTACA-CATGGCTGACTGGTACCTCCCTGGCCTCTCA-3′. PTS1 deletion constructs were created by amplifying full-coding

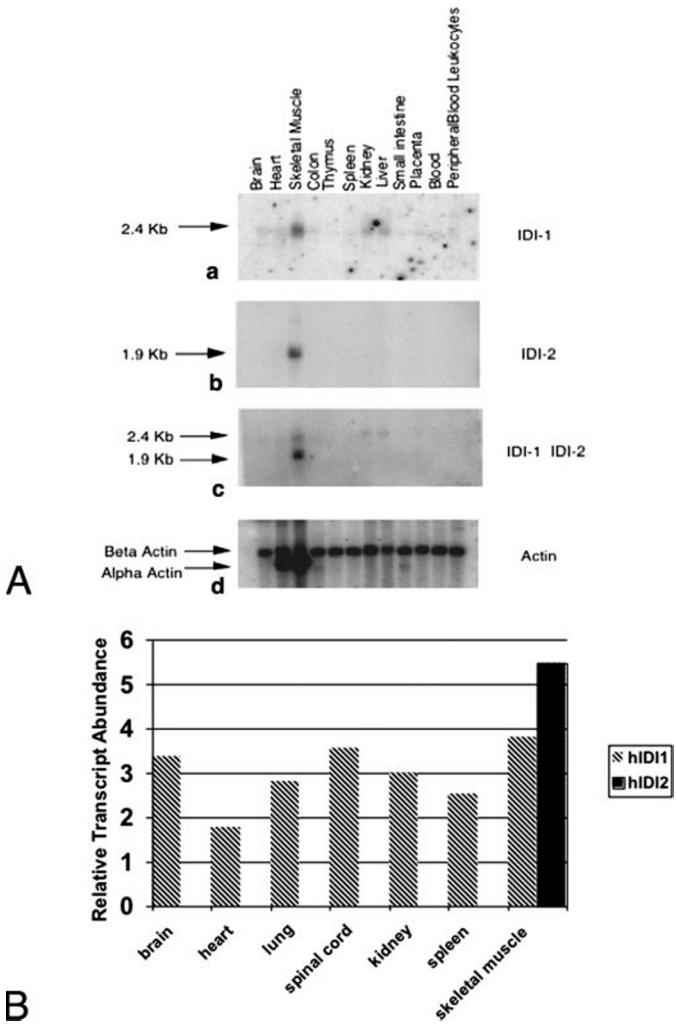

FIGURE 1. **Northern analysis and QRT-PCR of IDI1 and IDI2.** *A*, multiple tissue Northern blot (Clontech) containing 2 μg of poly(A) RNA per lane. *Panel a*, probed for IDI1; *panel b*, probed for IDI2; *panel c*, probed simultaneously for IDI1 and IDI2; *panel d*, ^{32}P-labeled actin cDNA probe hybridized to the same blot to ensure equal loading of samples. α-Actin, the predominate actin isoform, hybridizes in sample lanes of heart and skeletal muscle. *B*, QRT-PCR analysis of mRNA transcript expression from a variety of human tissues indicates that hIDI2 is expressed at detectable levels only in skeletal muscle. In contrast, hIDI1 is expressed in all tissues examined.

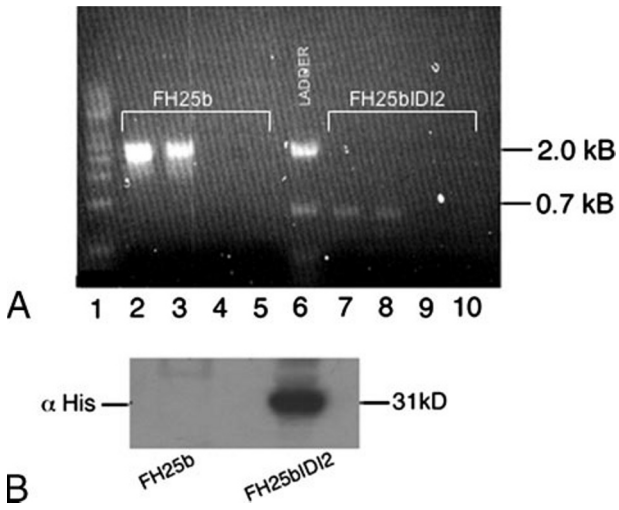

FIGURE 2. **pYESIDI2 is efficiently shuffled into FH25b.** *A*, yeast colony PCR analysis shows the presence of IDI1 (*lanes 2* and *3*) and absence of IDI2 (*lanes 4* and *5*) in FH25b haploid yeast. In contrast, IDI2 is present in (*lanes 7* and *8*) and IDI1 is absent in FH25bIDI2 (*lanes 9* and *10*). *Lanes 1* and *6* contain DNA ladders for size reference. *B*, Western blot analysis of FH25b and FH25bIDI2 (soluble extract, 30 μg) illustrates the absence of a 31-kDa IDI2 in the FH25b extract and the presence of the 31-kDa IDI2 in the FH25bIDI2 extract with α-His antibody (Roche Applied Science).

region template with reverse primers that added a unique KpnI restriction site and a TGA stop codon upstream of the final 3 amino acids IDI1ΔPTS1rev 5′-GTAATCAGGTACCTACATATTCACATTCTTCATATTTTCTC-3′ and IDI2 ΔPTS1rev-5′-TGGCTGACTGGTACCTCCCTGGCCTCTCACACTCTTCATAT-3′.The amplification products were subcloned into pCR4-TOPO (Invitrogen). The fragments were excised by restriction digest with BglII and KpnI. The excised fragments were cloned into pEGFP-C3 (Clontech). The recombinant pEGFP constructs were then determined to be in-frame with the N-terminal EGFP, and the PTS1 deletions were confirmed in triplicate by DNA sequencing.

Fluorescence Microscopy—Transfected cells were grown on collagen-coated glass coverslips. 24 h post-transfection cells were fixed in 4% paraformaldehyde in phosphate-buffered saline. Coverslips were mounted on glass slides in Mowiol 4–88 (Calbiochem) with 0.5% *n*-propylgallate as anti-fade agent. Fluorescence was visualized using confocal micoscope (Leica).

Quantitative Colocalization Analysis—Confocal images were transferred to a Macintosh PowerPC G4 (Apple Computer, Cupertino, CA) for analysis. Colocalization of fluorescent signal was evaluated quantitatively for Pearson's correlation coefficient (R_r), Manders overlap coefficient using CoLocalizer Express (CoLocalizer Express Software, Boise, ID). At least three samples from each experiment were analyzed. Data were prepared as Excel and Image files. Microsoft Excel software was used to analyze Excel files.

Animals—Mice, for each treatment group, were age-matched male Black Swiss (Taconic), a cross between C57/BL6 and Swiss Webster ($n = 5$, for each treatment). Mice were sacrificed at ~100 days of age, following the completion of experimental protocols. Tissues were immediately harvested, flash-frozen in liquid nitrogen, and stored at −70 °C.

Mice Diets—All diets were administered for 30 days, *ad libitum*. HFD was Harlan Teklad's special 1.25% cholesterol diet (TD96335). The statin diet was prepared with 0.1% simvastatin (Sigma-Aldrich). The fibrate diet was prepared with 0.2% gemfibrozil (Sigma-Aldrich).

Quantitative Real-Time PCR—The mRNA levels were quantitated using a Bio-Rad iCyler. iQ SYBR Green supermix (Bio-Rad) was used for all experiments. Experiments were done on 96-well plates (Axygen, Union City, CA). Each sample was run in triplicate and normalized to glyceraldehyde-3-phosphate dehydrogenase (GAPDH). The following primers were used: Mouse IDI1 Forward: 5′-GGTTCAGCTTCTAGCGGAGA-3′ and Reverse: 5′-TCGCCTGGGTTACTTAATGG-3′; Mouse IDI2 Forward: 5′-GATTGGCTACCTTCTGTTG-3′ and Reverse: 5′-CTGAACCAAGGGGTGATC-3′; Mouse HMGCR Forward: 5′-CTTGTGGAATGCCTTGTGATTG-3′ and Reverse: 5′-AGCCGAAGCAGCACATGAT-3′; Mouse GAPDH

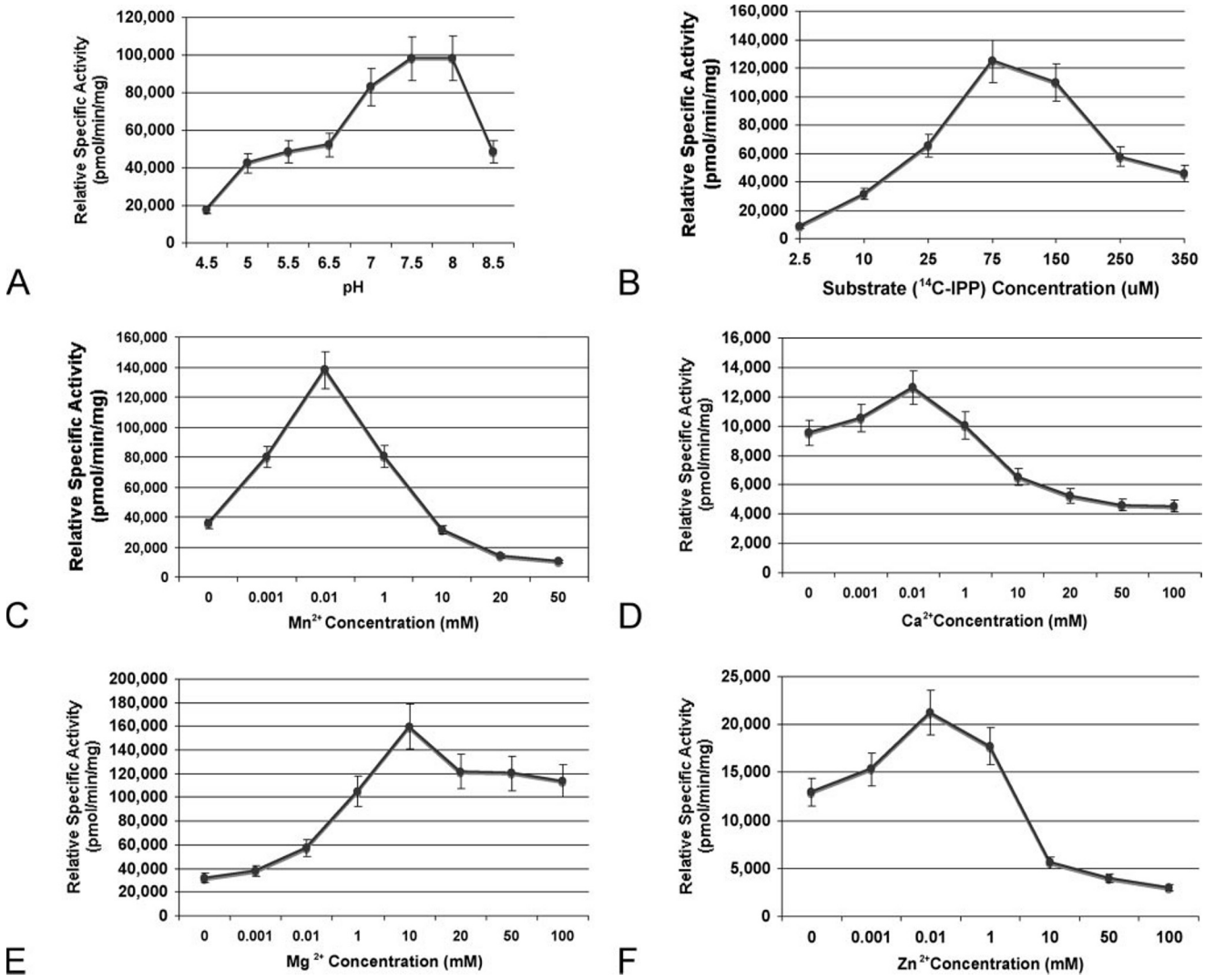

FIGURE 3. **Kinetic profile of human IDI2.** Partially purified IDI2 was tested for isomerase activity under conditions of increasing pH (4.5–8.5) (*A*), substrate (2.5-350 μM [^{14}C]IPP) (*B*) and in the presence of different divalent metal cofactors including Mn^{2+}, Ca^{2+}, Mg^{2+}, and Zn^{2+} (*C–F*). The assay was determined to be linear for protein and incubation times. Results are the mean ± S.D. of three experiments.

Forward: 5′-GTGTCCGTCGTGGATCTGA-3′ and Reverse: 5′-CAAGAAGGTGGTGAAGCAGG-3′.

Mammalian Expression Vectors—Murine IDI1 and IDI2 cDNA was obtained using SuperScript, oligo(dT) primer, and total RNA according to the manufacturer's protocol. IDI2 was amplified from mouse neonate skeletal muscle cDNA with the following primers: 5′-CGGCGCTAGCACCATGGGATTTC-CAGGCAAGCAAAACTCACCTT and 3′-CGGTCAAGA-TCACAGTCCATATATCTTGTCAGGCTCCAC.

Cell Culture and Transfection Conditions—HeLa cells were maintained in Eagles Minimum Essential Medium (EMEM) (Invitrogen) containing 10% fetal bovine serum (Life Technologies), penicillin (100 units/ml), and streptomycin sulfate (100 μg/ml) at 37° under 5% CO_2. The mouse myoblast cell line C_2C_{12} (American Tissue Culture Collection) was grown in Dulbecco's modified Eagle's medium (Invitrogen) supplemented with 1 mM sodium pyruvate, 10% fetal bovine serum (Sigma-Aldrich), and fungizone and streptomycin. Cells were transected using Lipofectamine 2000 (Invitrogen). Overexpression of IDI2 in C_2C_{12} cells was verified by real-time quantitative RT-PCR.

Cholesterol Synthesis Assay—Cholesterol, fatty acid, and dolichol phosphate rate of synthesis was determined using the method previously described (13) with the following modifications: 100-mm cell culture plates were seeded with 2×10^5 C_2C_{12}-transfected cells with either vector-only or pcDNA3.1IDI2 vector. After 24 h, plates were rinsed 3× in phosphate-buffered saline. Cells were incubated in LPDS medium for 24 h.

Cellular Cholesterol Determination—Total cholesterol levels were determined by Michael J. Richards and Dr. Steven Fliesler (St. Louis University School of Medicine, St. Louis, MO) using reverse-phase high-performance liquid chromatography (HPLC) after saponification and petroleum ether extraction, as described previously (14, 15).

HMGCR Assay—HMGCR activity in C_2C_{12} cells was determined as previously described (16), with the following modifications: activity in the cellular extract was determined using 100 μg of protein, incubated for 1 h at 37 °C.

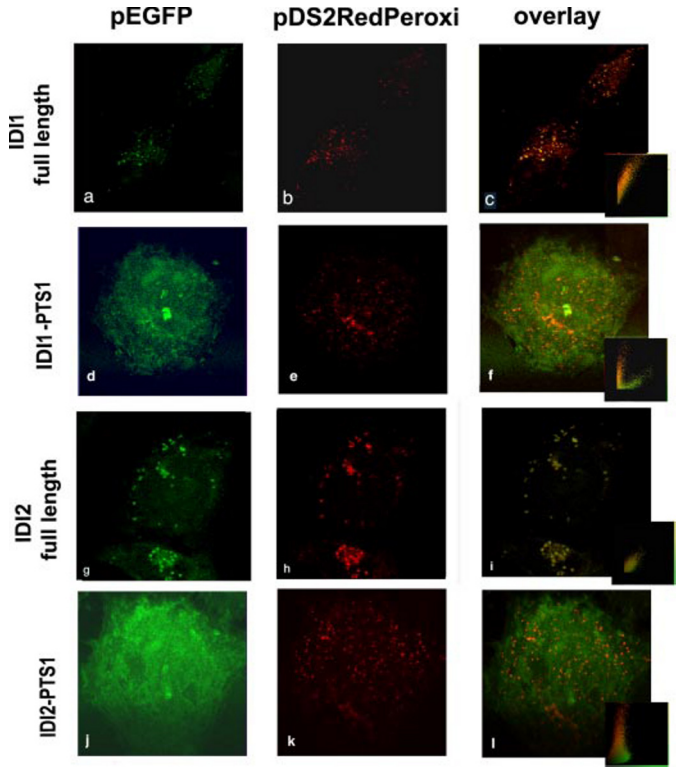

FIGURE 4. **Subcellular localization of hIDI1 and hIDI2.** Subcellular localization in HeLa cells of full-length EGFP fusions of IDI1 and IDI2 (*panels a* and *g*) and PTS1-deleted constructs (*panels d* and *j*). Punctate fluorescent pattern is indicated by expression of DSRed2-peroxi in the same cells (*panels b*, *e*, *h*, and *k*). Peroxisomal colocalization of full-length IDI1 and IDI2 constructs is verified by colocalization of the two images (*panels c* and *i*). Overlay images indicate that deletion of C-terminal PTS1 for both IDI1 and IDI2 eliminates peroxisomal targeting (*panels f* and *l*). The embedded scattergrams generated by co-localization software (Co-localizer Express) indicates relative distribution of each fluorophore (*lower right* of overlay images *panels c*, *f*, *i*, and *l*).

RESULTS

Tissue Distribution of IDI2—To determine the expression pattern of IDI2 in human tissues, a commercially prepared multiple tissue Northern blot (Clontech) was probed against both IDI1 and IDI2 ^{32}P-labeled cDNA (Fig. 1*A*). IDI1 expression is shown as a 2.4-kb transcript detectable in brain, heart, skeletal muscle, kidney, and liver (Fig. 1*A*, *panel a*). In contrast, IDI2 is expressed as a 1.9-kb transcript that is detectable exclusively in skeletal muscle (Fig. 1*A*, *panel b*). Simultaneous probing indicates that IDI2 is expressed at a notably higher level than IDI1 in skeletal muscle (Fig. 1*A*, *panel c*). These data were confirmed in a variety of human tissues using quantitative real-time PCR (QRT-PCR) (Fig. 1*B*). In agreement with Northern data, the QRT-PCR data illustrate that IDI2 is present only in skeletal muscle and expressed at higher levels than IDI1.

hIDI2 Functional Complementation of IDI1 in S. cerevisiae—The significant sequence similarity of the two isozymes, at both the amino acid and nucleotide level, led us to predict that IDI2 may retain functional isomerase activity despite a C86S change within the putative active site (10). As described earlier, a C139S mutation in yeast, corresponding to the C86S in humans resulted in an inefficient yet still active enzyme. To investigate the *in vivo* isomerase activity of IDI2 we tested the ability of hIDI2 to functionally rescue a non-functional IDI1 by the plasmid shuffle technique (18). IDI1 is an essential single copy gene in yeast, therefore the loss of episomal pRS317:IDI1 in the yeast strain FH25b is lethal unless functionally complemented by hIDI2. We were able to obtain transformants for IDI2 but were unsuccessful in recovering transformants for human IDI1. We confirmed the presence or absence of pRS317:IDI1 or pYES IDI2 in the positive shuffle transformants by PCR (Fig. 2*A*). Yeast colony PCR analysis shows the presence of IDI1 (*lanes 2* and *3*) and absence of IDI2 (*lanes 4* and *5*) in FH25b haploid yeast. In contrast, IDI2 is present (*lanes 7* and *8*), and IDI1 is absent in FH25bIDI2 (*lanes 9* and *10*). Western analysis of the soluble protein extracts demonstrates that a 31-kDa His-tagged IDI2 is expressed at high levels in FH25bIDI2 but not in FH25b (Fig. 2*B*). These results demonstrate that human IDI2 is functionally homologous to yeast IDI1.

Kinetic Analysis of Recombinant Full-length Human IDI2 in FH25b—To determine the kinetic parameters of IDI2, we utilized the recombinant yeast strain FH25bIDI2 generated by plasmid shuffle, which is devoid of endogenous yeast IDI1. Partially purified IDI2 extracts were assayed *in vitro* for isomerase activity. Kinetic analysis indicates hIDI2 has maximal activity at pH 8.0 (Fig. 3*A*). Thus, all subsequent assays were carried out at pH 8.0. Our data show the optimal substrate concentration for IDI2 is 75 μM [^{14}C]IPP (Fig. 3, *panel B*). Thus, the maximal relative specific activity for hIDI2 is $1.2 \times 10^{-1} \pm 0.3$ μmol min^{-1} mg^{-1} at pH 8.0 with a K_m^{IPP} value of 22.8 μM IPP.

Previous characterization of IDI1 in yeast showed that for maximum biological activity the enzyme requires a divalent metal as a cofactor (18). In addition, recently it has been shown that IDI1 isolated from *E. coli* has two metal binding sites; one site binds Mg^{2+} while the other is hypothesized to bind a Zn^{2+} atom (19). To determine the requirement for metal cofactors for hIDI2 we measured the *in vitro* activity of hIDI2 in the presence of several divalent metals (Fig. 3, *C–F*). Our data indicate that highest maximal activity for IDI2 is seen at concentrations of 0.01 mM Mn^{2+}. These results suggest Mn^{2+} may be the physiologically important cation for IDI2 (Fig. 3*C*).

Subcellular Localization of hIDI2—IDI1 cloned from rat and hamster is localized to the peroxisome by a PTS1-dependent pathway (5). Human IDI1 has a putative C-terminal PTS1 (-YRM) which conforms to the "two out of three" rule for the adherence to the canonical consensus sequence for peroxisomal targeting (20). Similarly, the sequence of human IDI2 contains a less stringent C-terminal PTS1 (-HRV). Previously, it has been shown that many non-canonical tripeptide combinations were able to target the enzyme malate dehydrogenase in *S. cerevisiae* to the peroxisome (20).

To determine the requirement for peroxisomal localization of the putative PTS1 at the C terminus of human IDI1 and IDI2, we generated EGFP fusion proteins of human IDI1 and IDI2, both as full-length and C-terminal tripeptide PTS1 deletion constructs. HeLa cells were co-transfected with the fusion constructs as well as the vector DsRed2peroxi. This vector contains the coding sequence of the red fluorescent protein DsRed1 from *Discosomas p* followed by a C-terminal peroxisomal targeting sequence, SKL.

Transient transfection of full-length IDI1-EGFP and IDI2-EGFP fusion constructs into HeLa cells resulted in a punctate expression pattern that was superimposable with the punctate

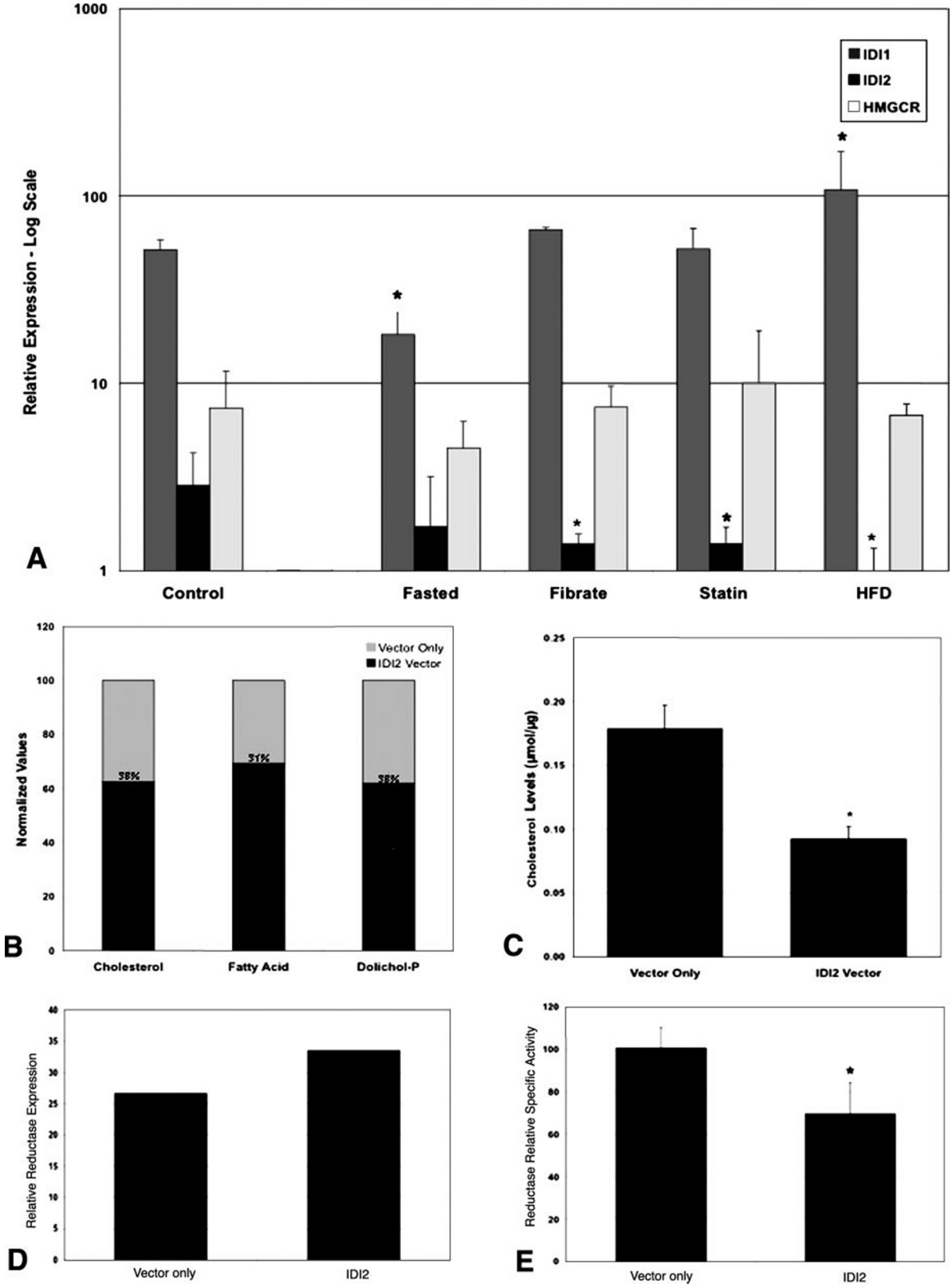

FIGURE 5. **IDI1, IDI2, and HMGCR regulation in mouse muscle and effects on the isoprenoid pathway in IDI2 overexpressed C_2C_{12} cells.** *A*, QRT- PCR analysis of mRNA expression levels of IDI, IDI2, and HMGCR in murine muscle following treatment with fibrate (gemfibrozil), statin (simvastatin), high fat diet (*HFD*), or fasting. Relative expression is measured compared with untreated control mice ($n = 5$). Results are the mean ± S.D. of three experiments. Mann-Whitney *U* test for significance indicates (*) $p \leq 0.05$. *B*, rate of cholesterol, dolichol, and fatty acid biosynthesis was decreased 38, 31, and 38%, respectively in IDI2-overexpressing cells compared with C_2C_{12} cells stably transfected with pcDNA3.1(-) vector only. *C*, total cellular cholesterol levels were determined by reverse-phase HPLC and the in murine IDI2-overexpressing cells. *D*, HMGCR mRNA levels of mIDI2 cells were statistically unchanged compared with pcDNA 3.1(-) vector-transfected control cells. *E*, HMGCR activity determinations in stably transfected IDI2 C_2C_{12} cells and vector-only cells. Relative activity is measured compared with vector control cells. Results for all panels are the mean ± S.D. of three experiments. Student's *t* test for significance indicates (*) $p \leq 0.05$.

pattern generated by pDsRed2peroxi in the same cell (Fig. 4, *panels a–c*, *panels g–i*). Moreover, correlation values (Pearson, R_r and Manders, *R*) indicate a significant degree of colocalization for both EGFPIDI1/DsRed2peroxi (R_r = 0.9098, r = 0.9099) and EGFPIDI2/DsRed2peroxi (R_r = 0.9454, r = 0.9454). Scatter plots (embedded in *lower right* of Fig. 4, *panels c* and *i*) estimate the amount of detected fluorescence based on localization of DsRedperoxi (*red*, *y*-axis) and EGFP (*green*, *x*-axis). Colocalized pixels (*yellow*) are located along the diagonal of the scatter gram. The scatter plots for full-length EGFP-IDI1 and EGFP-IDI2 indicate a yellow monopartite diagonal scatter pattern, which verifies the colocalization of both IDI1 and IDI2 with targeted DS2peroxi to peroxisomes.

In contrast, transient transfections of the EGFP-PTS1 deletion constructs in HeLa cells resulted in a diffuse fluorescent pattern, which was cytosolic in distribution (Fig. 4, *panels d* and *j*), while the fluorescent pattern for DsRed2peroxi remained punctate (Fig. 4, *panels e* and *k*). Furthermore, superimposed images indicate that PTS1 deletions in IDI1 and IDI2 obviate co-localization with DsRed2peroxi (Fig. 4, *panels f* and *l*).

Colocalization correlation values for both EGFPIDI1ΔPTS1/DsRed2peroxi and EGFPIDI2ΔPTS1/DsRed2peroxi co-transfected cells were greatly reduced compared with values for full-length constructs (R_r = 0.3099. r = 0.3098; R_r = 0.2671, r = 0.2670). Scatter plots for ΔPTS1-expressing cells (*panels f* and *l*, *embedded lower right*) show a bipartite distribution along the x (*green*, EGFP) and y (*red*, DsRed2peroxi) axes, indicating extremely low levels of colocalization. Taken together, these data demonstrate the localization of full-length human IDI1 and IDI2 to peroxisomes and show that this targeting is mediated by C-terminal PTS1 sequence.

Regulation of IDI2 in Mice—The muscle-specific expression of IDI2 in combination with demonstrable isomerase activity led us to hypothesize that IDI2 may play a unique role in the isoprenoid pathway in muscle. Our previous work suggested that IDI2 may be a factor in muscle-specific pathologies, such as rhabdomyolysis stemming from treatment with statins (simvastatin), a class of cholesterol-lowering drugs that act specifically as HMG-CoA reductase (HMGCR) inhibitors (10).

To address the effect on IDI2 transcription in skeletal muscle in the presence of statins, we measured mRNA levels of IDI1, IDI2, and HMG-CoA reductase (HMGCR) by quantitative real time PCR (QRT-PCR) in murine muscle tissue (hind limb). mRNA levels were measured following treatment with statins as well as fibrates, another class of cholesterol-lowering drugs that has been shown to cause rhabdomyolysis in some patients (21). Additionally we measured the effect on IDI1, IDI2, and HMGCR mRNA levels following high fat (HFD) and fasted diets. Modified dietary regimes, including high fat and fasted diets, have been shown to modulate transcription of genes involved in isoprenoid and lipid metabolism in skeletal muscle (22, 23).

Our data demonstrate that IDI2 mRNA levels were significantly reduced under statin (51% $p < 0.05$) and fibrate (51% $p < 0.05$) treatments (Fig. 5*A*). In contrast, mRNA levels of IDI1 and HMGCR were unchanged under either treatment (Fig. 5*A*). In addition, IDI2 mRNA levels in skeletal muscle following HFD were also significantly reduced (65%, $p \leq 0.05$) (Fig. 5*A*). In contrast, IDI1 transcription following HFD was significantly increased (209%, $p < 0.05$) (Fig. 5*A*). Measurements of mRNA transcription following a fasted regime demonstrate a significant down-regulation of IDI1 (65%, $p \leq 0.05$) (Fig. 5*A*). IDI2 and HMGCR transcription levels showed no significant change with this treatment. Taken together, these data suggest a regulatory difference for the three genes in skeletal muscle.

mIDI2 Overexpression in C_2C_{12} Cells—To further explore the function of IDI2, and address the effect of IDI2 overexpression on sterol and non-sterol products downstream of the isoprenoid pathway, mammalian expression constructs were designed to constitutively express murine IDI2. These constructs were stably transfected into mouse myoblast C_2C_{12} cells. The rate of sterol (cholesterol) and non-sterol (dolichols, fatty acids) biosynthesis was determined. The rate of cholesterol, fatty acid, and dolichol synthesis was decreased 38, 31, and 38%, respectively in IDI2-overexpressing cells compared with C_2C_{12} cells stably transfected with pcDNA3.1(-) vector-only (Fig. 5*B*). Furthermore, the amount of total cellular cholesterol in murine IDI2-overexpressing cells was also decreased (48%) as compared with vector-transfected control cells (Fig. 5*C*).

To address the mechanism for reduction of cholesterol by mIDI2 overexpression, we determined the level of HMGCR transcription as well as HMGCR activity in these cells. HMGCR mRNA levels in mIDI2-overexpressing cells were not significantly affected compared with vector-transfected control cells (Fig. 5*D*). However, mIDI2-overexpressing cells showed a significant reduction in HMGCR activity (31%, $p < 0.05$) (Fig. 5*E*). Taken together, these data suggest that IDI2 has a role in the modulation of downstream sterol and non-sterol products. Moreover, this regulation may be likely at the level of HMGCR activity inhibition.

We were unable to recover any viable murine IDI1 transformants in C_2C_{12} cells. These results are similar to our unsuccessful efforts to overexpress hIDI1 in *S. cerevisiae* and may reflect an intolerance in these cells for high levels of overexpressed IDI1in the presence of endogenous IDI1.

DISCUSSION

IDI2 shares a high degree of sequence homology to its isozyme IDI1 at both the amino acid and nucleotide level (10). The predicted protein product shows 81% similarity and 65% identity to human IDI1. IDI1 is ubiquitously expressed in all human tissues examined. In contrast, IDI2 is expressed only in skeletal muscle, suggesting a muscle specific function in isoprenoid metabolism.

To determine if IDI2 functions as an isomerase *in vivo*, IDI2 was overexpressed in yeast, and shown to functionally complement *idi1* yeast. Moreover, partially purified human IDI2, expressed in yeast, catalyzes the conversion of [^{14}C]IPP to [^{14}C]DMAPP *in vitro*. The kinetics indicate that IDI2 has a maximal relative specific activity of $1.2 \times 10^{-1} \pm 0.3$ μmol min^{-1} mg^{-1} at a pH 8.0 at 37 °C. This value is 34-fold lower than published values for human IDI1 expressed in *E. coli* (V_{max} 4.1 ± 0.1 μmol min^{-1} mg^{-1} at pH 7.0) (24). IDI2 shows maximal activity in the presence of 0.01 mM Mn^{2+}. Recombinant human IDI1 has maximum activity in the presence of 20 mM

Mg (11, 24). Thus, Mn^{2+} may play an important physiological role in IDI2 catalytic activity.

As mentioned previously, analysis of IDI1 in *S. cerevisiae* revealed two catalytically active amino acids, Cys^{139} (Cys^{86}, human) and Glu^{207} (Glu^{49}, humans). Mutagenesis analysis in the yeast enzyme demonstrated that a C139S mutation resulted in a significant reduction in isomerase activity but Cys→Val or Ala change at this site abolished activity completely (6). Activity analysis in our current study indicates that, in a yeast expression system, hIDI2, which retains the Glu^{149} critical residue but has a C86S change, has isomerase activity *in vitro*.

A model for catalytic activity in IDI2 was presented previously (10). We proposed that the exchange of Asn^{83} by Asp^{83} may sufficiently increase the acidity of Ser^{86} to enable protonation of IPP. In support of this, a recent study characterizing the crystal structure of the inactive C67A in *E. coli* complexed with the irreversible inhibitor EIPP, indicates that the protonation machinery is still intact and that Glu^{116} (Glu^{149} human) can function as an active nucleophile (25). While further studies are required to identify the IDI2 specific active site residues, our data show that IDI2 is capable of catalyzing the isomerization of IPP to DMAPP by a novel mechanism.

Further characterization of the two human isozymes demonstrates that both IDI1 and IDI2 are localized to the peroxisome by way of a PTS1-dependent import pathway. The C-terminal tripeptide deletions of the putative PTS1 sequences (-YRM, IDI1 and -HRV, IDI2) results in the loss of peroxisomal targeting. These results are not unanticipated in view of the recent evidence expanding the canonical C-terminal PTS1 tripeptide to include the residues {SAGCN}-{RKH}-{LIVMAF} (26). Importantly, it has also been shown that non-conserved substitutions of the −3 residue position are able to retain peroxisomal targeting (20). In addition, studies have determined that cryptic upstream auxiliary residues at positions −4 and −5 effect PTS1-Pex5p receptor binding affinities and thus peroxisomal import (27). Significantly, sequence analysis indicates that human IDI1 and IDI2 share complete amino acid homology at these positions with peroxisomal rat and hamster IDI1. While differences in subcellular localization of IDI in plants are thought to provide a mechanism for regulation of the various isoforms, our data suggest no such organizational mechanism exists for the IDI isozymes in humans. As a result, we expect that regulatory differences for IDI1 and IDI2 are likely to be at the promoter level. The existence of different genes encoding the same enzymatic activity can provide a mechanism by which isozymes in the same subcellular location can be independently regulated at the level of gene expression.

Dual subcellular localization of isoprenoid and lipid pathway enzymes have been reported previously (28, 29) Moreover, localization of isozymes to the same intracellular location is not unique. Both phosphatidylserine synthase 1 (PSS1) and PSS2 shown to synthesize phosphatidylserine are localized to the mitochondria-associated membranes (30).

Presently, the metabolic effect of dietary and cholesterol lowering regimes on the transcription of skeletal muscle genes in the mevalonate pathway remains uncharacterized. Our current study demonstrates that IDI2 is significantly affected under the cholesterol-lowering treatments statins and fibrates as well as HFD. Statins have been shown to upregulate liver fatty acid-binding protein (L-FABP) through PPARα, a class of nuclear transcription factors involved in regulation of lipid metabolism (31). Similarly, fibrates modulate synthesis of lipoprotein lipase and ApoA1 mediated by PPARα-dependent activation. Dietary modifications including HFD and fasting have also been implicated as activators PPARα (32). While further analysis is necessary, our data suggest that IDI2 transcription may be modulated by PPARα activation.

Regulation of HMGCR is complex and multifaceted and is known to occur at the transcriptional, translational, and post-translational level. Recent evidence suggests that non-sterol species including the C_{15} isoprenoid FPP or farnesol (FOH) may be regulators of HMGCR (33, 34, 35). Moreover, recent studies have indicated that FPP, which is inter-convertible with FOH, inhibits fatty acid synthesis in an SREBP-independent manner (36) The mechanism for the decrease in HMGCR activity and resultant decrease in the downstream products, cholesterol and dolichol, as well as a decrease in fatty acids in the IDI2 overexpressing C_2C_{12} cells may be through an increased pool of FPP and/or FOH. Moreover, FOH has been shown to induce activation of PPARα (35). Thus, the possibility exists that regulation of IDI2 may be through a feedback mechanism involving FPP and/or FOH production and PPARα activation in skeletal muscle.

In most instances investigated thus far, the presence of an alternative, substitute enzyme does not appear to be the sole reason for the existence of multiple isoforms of lipid-biosynthetic enzymes (29). The data suggest that one isoform cannot fully replace another (29). Therefore, enzyme duplication does not merely represent redundancy but, rather, that the different isoforms perform specific functions.

In summary, we have characterized a novel isozyme of isopentenyl diphosphate isomerase, IDI2. IDI2 differs from the previously characterized IDI1 in tissue distribution, kinetic parameters, and catalytic mechanism. Both isozymes are localized to the peroxisome, mediated by a non-canonical PTS1 sequence. In addition, it has been well established that IDI1, is regulated at the level of SREBP; in contrast, our data suggest that IDI2 may be regulated by a different mechanism, involving PPARα. The muscle-specific transcription of IDI2, in combination with the enzymes ability to modulate cholesterol biosynthesis, and produce HMGCR activity inhibition, makes IDI2 an interesting candidate for a cholesterol-lowering therapeutic target.

Acknowledgments—We thank Dr. Steve Barlow, SDSU Microscope Facility, for confocal microscopy assistance and Lisa Kwizera M.P.H., San Diego State University Foundation, for SSP statistical software analysis.

REFERENCES

1. Spurgin, S. L., and Porter, J. W. (1981) in *Biosynthesis of Isoprenoid Compounds* (Porter, J. W., and Spurgin S. L., eds) vol. 1, pp. 2–46. Wiley and Sons, Inc, New York
2. Barbacid, M. (1987) *Annu. Rev. Biochem.* **56,** 779–827
3. Popjak, G., (1970) in *Natural Substances Formed Biologically from Mevalonic Acid* (Goodwin, T.W., ed) pp. 17–33, Academic Press, New York

4. Lynen, F., Argranoff, B. W., Eggerer, H., Henning, U., and Moslein, F. M. (1959) *Angew. Chem.* **71,** 657–661
5. Paton, V., Shackelford, J. E., and Krisans, S. K. (1997) *J. Biol. Chem.* **272,** 18945–18950
6. Street, I. P., Coffman, H., Baker, J. A., and Poulter C. D. (1994) *Biochemistry* **33,** 4212–4217
7. Nakamura, A., Shimada, H., Masuda, T., Ohta, H., and Takamy, K. (2001) *FEBS Lett.* **506,** 61–64
8. Bruenger, E., Chayet, L., and Rilling, H. C. (1986) *Arch. Biochem. Biophys.* **248,** 620–625
9. Sagami, H., and Ogura, K. (1983) *J. Biochem.* (*Tokyo*) **94,** 975–979
10. Breitling, R., Laubner, D., Clizbe, D., Adamski, J., and Krisans, S. K. (2003) *J. Mol. Evol.* **57,** 282–291
11. Hahn, F. M., Xuan, J. W., Chambers, A. F., and Poulter, C. D. (1996) *Arch. Biochem. Biophys.* **332,** 30–34
12. Satterwhite, D. M. (1985) *Methods Enzymol.* **110,** 92–99
13. Aboushadi, N., and Krisans, S. K. (1998) *J. Lipid Res.* **39,** 1781–1791
14. Fliesler, S. J., Richards, M. J., Miller, C., and Peachey N. S. (1999) *Investig. Ophthalmol. Vis. Sci.* **40,** 1792–1801
15. Fliesler, S. J., Richards, M. J., Miller, C. Y., and Cenedella, R. (2000) *J. Lipids* **35,** 289–296
16. Engfelt, W. H., Shackelford, J. E., Aboushadi, N., Jessani, N., Masuda, K., Paton, V. G., Keller, G. A., and Krisans, S. K. (1997) *J. Biol. Chem.* **272,** 24579–24587
17. Durbecq, V., Sainz, G., Oudjama, Y., Clantin, B., Bompard-Gilles, C., Tricot, C., Caillet, J., Stalon, V., Droogmans, L., and Villeret, V. (2001) *EMBO J.* **20,** 1530–1537
18. Hahn, F. M., and Poulter, C. D. (1995) *J. Biol. Chem.* **270,** 11298–11303
19. Carrigan, C. N., and Poulter, C. D. (2003) *J. Am. Chem. Soc.* **125,** 9008–9009
20. Elgersma, Y., Vos, A., van den Berg. M., van Roermund, C. W. T., van der Sluijs, P., Diste, B., and Tabak, H. (1996) *J. Biol. Chem.* **271,** 26357–26382
21. Brunmair, B., Lest, A., Staniek, K., Gras, F., Scharf, N., Roden, M., Nohl, H., Waldhausl, W., and Furnsinn, C. (2004) *J. Pharmacol. Exp. Ther.* **311,** 109–114
22. Hildebrandt, A. L., and Neufer, P. D. (2000) *Am. J. Physiol. Endocrinol Metab.* **278,** E1078–E1086
23. Cameron-Smith, D., Burke, L. M., Angus, D. J., Tunstall, R. J., Cox, G. R., Bonen, A., Hawley, J. A., and Hargreaves, M. A. (2003) *Am. J. Clin. Nutr.* **77,** 313–318
24. Hahn, F. M., Hurlburt, A. P., and Poulter, C. D. (1999) *J. Bacteriol.* **181,** 4499–4504
25. Wouters, J., Oudjama, Y., Stalon, V., Droogmans, L., and Poulter, C. D. (2004) *Proteins* **54,** 216–221
26. Neuberger, G., Maurer-Stroh, S., Eisenhaber, B., Hartig, A., and Eisenhaber, F. (2003) *J. Mol. Biol.* **328,** 581–592
27. Maynard, E. L., Gatto, G. J., Jr., and Berg, J. M. (2004) *Proteins* **55,** 856–861
28. Kovacs, W. J., Olivier, L. M., and Krisans, S. K. (2002) *Prog Lipid Res.* **41,** 369–391
29. Vance, J. E. (1998) *Trends Biochem. Sci*. **23,** 423–428
30. Vance, J. E., and Vance, D. E. (2004) *Biochem. Cell Biol*. **82,** 113–128
31. Landrier, J. F., Thomas, C., Grober, J., Duez, H., Percevault, F., Souidi, M., Linard, C., Staels, B., and Besnard, P. (2004) *J. Biol. Chem.* **279,** 45512–45518
32. Spriet, L. L., Tunstall, R. J., Watt, M. J., Mehan, K. A., Hargreaves, M., and Cameron-Smith, D. J. (2004) *Appl. Physiol*. **96,** 2082–2087
33. Meigs, T. E., Roseman, D. S., and Simoni, R. D. (1996) *J. Biol. Chem.* **271,** 7916–7922
34. Meigs, T. E., and Simoni, R. D. (1997) *Arch. Biochem. Biophys*. **345,** 1–9
35. Holstein, S. A., and Hohl, R. J. (2004) *Lipids* **39,** 293–309
36. Murthy, S., Tong, H., and Hohl, R. J. (2005) *J. Biol. Chem.* **280,** 41793–41804